Acta Geophysica (2020) 68:51–73
https://doi.org/10.1007/s11600-019-00390-3

RESEARCH ARTICLE - SOLID EARTH SCIENCES

Possibility of an earthquake prediction based on monitoring crustal deformation anomalies and thermal anomalies at the epicenter of earthquakes with oblique thrust faulting

Zahra Alizadeh Zakaria[1] · **Farshid Farnood Ahmadi**[1]

Received: 26 April 2019 / Accepted: 30 November 2019 / Published online: 6 December 2019

Abstract
Is it possible to predict location, time and magnitude of earthquakes through identifying their precursors based on remotely sensed data? Earthquakes are usually preceded by unusual natural incidents that are considered as earthquake precursors. With the recent advances in remote sensing techniques which have made it possible monitoring the earth's surface with different sensors, scientists are now able to better study earthquake precursors. Thus, the present study aims at developing the algorithm of classic PS-InSAR processing for obtaining crustal deformation values at the epicenter of earthquakes with magnitude larger than 5.0 on the Richter scale and with oblique thrust faulting and then after calculating temperature values using remotely sensed thermal imagery at the epicenter of same earthquakes; thermal and crustal deformation anomalies were calculated using data mining techniques before earthquake occurrence. In the next stage, taking the correlation between thermal anomalies and crustal deformation anomalies at the epicenter of the study earthquakes into account, an integrated technique was proposed to predict probable magnitude and time of oblique thrust earthquakes occurrence over the earthquake-prone areas. Eventually, the validity of the proposed algorithm was evaluated for an earthquake with a different focal mechanism. The analysis results of the thermal anomalies and crustal deformation anomalies at the epicenter of April 16, 2016, Japan-Kumamoto earthquake of magnitude 7.0 with strike-slip faulting, showed completely different trends than the suggested patterns by the proposed algorithm.

Keywords Crustal deformation anomalies · Data mining · Earthquake precursors · Earthquake prediction · Extended-PS method · Surface thermal anomalies

Introduction

Earthquake prediction with purposes of reducing death and destruction caused by earthquakes is a significant issue that has attracted the attention of many experts and researchers in the field of disaster management (Tsai and Chen 2010; Rikitake 1968). While most seismologists insist on the improbability of earthquake prediction in terms of location and time of occurrence using the current knowledge and facilities, they believe that there are certain precursors that may lead to finding more reliable methods by investigating them effectively (Rikitake 1975). Therefore, considering the significance of this issue, extensive researches from various scientific fields have been concentrated on identifying these precursors. The most common predictive methods based on identifying precursors include monitoring the ground displacement along a fault using ground-based tools such as global positioning systems (GPS) (Yue and Lay 2011; Wang et al. 2013; Calais et al. 2003) or radar interferometry on radar images of satellite sensors (Tomás et al. 2014; Moro et al. 2017; Graham 1974; Bamler and Hartl 1998; Gabriel et al. 1989; Massonnet and Feigl 1998), earthquake prediction using geophysical techniques such as determining probable location or, sometimes, probable time of earthquake occurrence through foreshocks (Ogata and Katsura 2012; Moreno et al. 2010; Lippiello et al. 2012), earthquake prediction by means of assessing variations in velocity of seismic waves of S and P prior to earthquake (Pio Lucente et al. 2010; Peacock et al. 1988), earthquake prediction through monitoring thermal anomalies on the earth surface using

✉ Farshid Farnood Ahmadi
f.farnood.tabrizu@iran.ir

[1] Department of Geomatics Engineering, University of Tabriz, 29 Bahman Boulevard, Tabriz, Iran

thermal images obtained by remote sensors in fault-exposed areas (Pulinets et al. 2006; Saraf et al. 2009; Saradjian and Akhoondzadeh 2011), monitoring changes in ionospheric precursors analyzing the collected data from remote sensing DEMETER satellites (Molchanov et al. 2006; Akhoondzadeh et al. 2010) or ground-based systems (Yao et al. 2012; Pulinets and Davidenko 2014), earthquake prediction through monitoring earthquake clouds along fault range with the aid of satellite imagery (Thomas et al. 2015; Guo and Wang 2008), earthquake prediction using geochemical and hydrological precursors like monitoring variations in concentration of ions or dissolved gases including radon, helium, etc. (Thomas 1988; Ingebritsen and Manga 2014), earthquake prediction through studying changes in animal behaviors (Grant et al. 2015) and earthquake prediction by measuring electromagnetic changes in ULF range (Hayakawa 2013; Han et al. 2011).

Most of the above-mentioned methods require the installation of the equipment on the ground or direct contact with the ground. Since the long-term surveying installations within an area are time- and cost-consuming, the remote sensing techniques such as monitoring thermal anomalies and land surface deformation prior to earthquake within earthquake-prone areas using satellite images are of higher priority because they do not need physical presence at the site, and also the required data are continuously collected from a wider range with high spatiotemporal resolution and lower costs. But, remote sensing methods, similar to other predictive approaches, have a single-parametrical orientation toward the issue. On the other hand, since the inherent behavioral variations of the precursors don't follow a common pattern in all earthquakes, and the changes show peculiar behaviors to each region, it seems unfeasible to provide an obvious prediction in an area solely based on behavioral variations in a single precursor. Even in the case of the studies which have focused on investigating several precursors simultaneously, the correlation among latent structural patterns in the collected data related to different precursors has been ignored. Thus, these methods are not able to provide a reliable prediction about the location and time of earthquakes. However, these limitations never underestimate the precursors. Besides, since each precursor contains some information about earthquakes, it seems more likely to find an effective technique or an acceptable indicator for earthquake prediction. Therefore, the present study aims at developing the algorithm of classic PS-InSAR processing for obtaining crustal deformation values at the epicenter of earthquakes with magnitude larger than 5.0 on the Richter scale and with oblique thrust faulting, and then after calculating temperature values using remotely sensed thermal imagery at the epicenter of same earthquakes; thermal and crustal deformation anomalies were calculated using data mining techniques in the period of two months before earthquake occurrence; then, similarities or discrepancies among behavioral variations of these anomalies were analyzed. In the next stage, this approach was initially carried out in a unidimensional mode and then in an integrated form to offer a certain reliable method to predict the probable magnitude and time of earthquake based on identifying thermal anomalies and crustal deformation anomalies within earthquake-prone regions. Eventually, the validity of the proposed algorithm was evaluated for an earthquake with a different focal mechanism. The analysis results of the thermal anomalies and crustal deformation anomalies at the epicenter of April 16, 2016, Japan-Kumamoto earthquake of magnitude 7.0 with strike-slip faulting, showed completely different trends than the suggested patterns by the proposed algorithm. So the proposed algorithm was unable to determine the probable time and magnitude of an earthquake occurrence with strike-slip faulting.

Methodology

Recognition of the earthquake-prone areas

It should be noted that the remote sensing approaches to monitoring anomalies caused by earthquake precursors carry out the monitoring operation globally and over a wide area. Therefore, this issue comes into question that to monitor anomalies caused by earthquake precursors, which areas of the earth surface have to be monitored? In the present study, thermal anomalies and crustal deformation anomalies have been monitored regarding the already happened earthquakes. In other words, the epicenter of earthquakes to perform analyses was already identifiable. According to serious incidents, earthquake-prone areas are usually preceded by some turbulences such as minor shocks in the area, which are completely random and do not follow a certain pattern or principle, whereas the predictive locations of such shocks follow a certain order despite the high level of irregularity. But, it would be possible to estimate the probable location of earthquakes using modern statistical techniques like self-organizing map (SOM) neural networks (Mohankumar and Sangeetha 2018). This method is not only capable of identifying risky regions but also can give ideas about places that are vulnerable to earthquakes. As discussed above in the present study, the epicenter of earthquakes to perform analyses was already identifiable, but for evaluating the ratability of SOM networks to recognize earthquake-prone areas, we applied the SOM algorithm for identifying earthquake-prone areas in one of the study areas, whose stages are depicted in detail in Fig. 1.

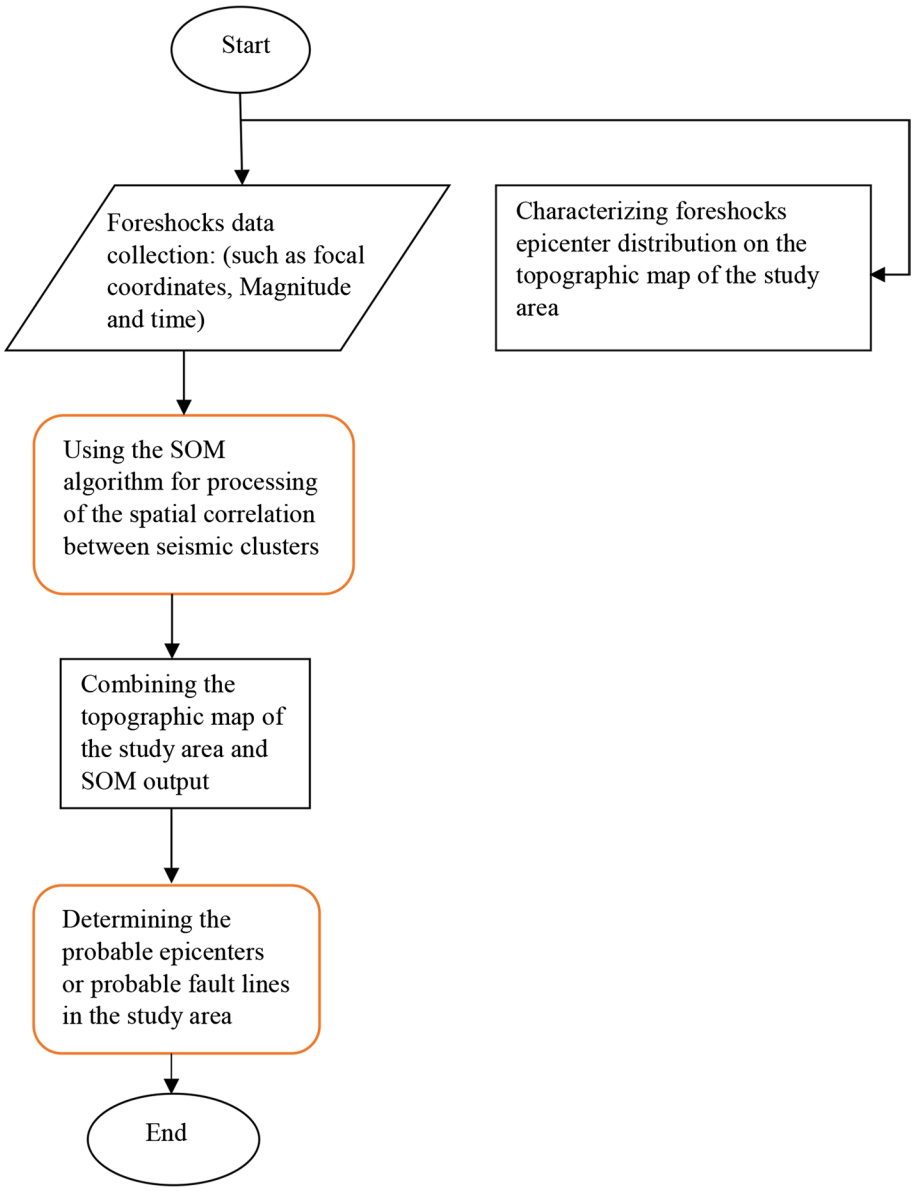

Fig. 1 SOM algorithm for analyzing spatiotemporal correlation between seismic clusters

Calculation of the crustal deformation anomalies at the epicenter of an earthquake

Monitoring of the ground surface deformations at the epicenter of an earthquake using radar interferometry

Ground surface deformations are considered as one of the direct impacts caused by tension exerted on the rocks, so by measuring length and width of a certain region of the ground surface located on an active plate, it is possible to map movements of the plate in relation to time, which can play a significant role in predicting earthquake probable time and location (Parsons 2017; Huang et al. 2017). A wide range of methods has been developed so far to measurement crustal movements. However, using radar interferometry technique has some advantages over other methods due to its wide coverage over ground surface, repeatability of observations over time, high spatiotemporal resolution and saving time and costs (Bürgmann et al. 2000; Rosen et al. 1998; Massonnet et al. 1993; Peltzer and Rosen 1995).

Advanced techniques of InSAR involving the simultaneous processing of multiple SAR acquisitions in time increase the number of locations where a deformation signal can be extracted and reduce associated error. Currently, there are two broad categories of algorithms for processing multiple acquisitions, persistent scatterer (PS-INSAR) and small baseline methods (SBAS), which are optimized for different models of scattering. Each of these two methods gives temporal solution to the uncorrelated phenomena based on the

principle of dominant reflectivity of centers of permanent scatterers (Hooper 2008). Considering that the SBAS technique relies on an appropriate combination of differential interferograms created by using image pairs characterized by a small orbital separation (baseline), using of the SBAS method leads to low spatial decorrelation results. Therefore, in the present study according to the PS method (Tu et al. 2012) which uses large stacks of SAR images to generate differential interferograms concerning common one master, we used classic PS-InSAR principles in our analyses. But classic PS technique to calculate the displacements of selected points faces this restriction that the amount of displacements is only measurable at the PS points around our study area which may not correspond to the target points (e.g., Earthquake epicenter). Thus, the classic PS method was not responsive to the purpose of this study to monitoring surface deformations of the earthquake's epicenter. So considering the limitations of the classic PS method due to lack of concentration on a selective point with specific geographical coordinates, in the present study the problem of determining the displacements at the selective points has been solved through spatiotemporal interpolation methods (Li and Heap 2014; Yang et al. 2004) based on calculated displacements for the PS points, whose stages are depicted in detail in Fig. 2a.

Behavioral analysis of the earthquake epicenter deformations and calculating crustal deformation anomalies using data mining

In the presented study, data mining methods (Hand 2007) were used to analyze the behavior of the crustal deformations at the epicenter of the earthquakes in order to calculate crustal deformation anomalies.

It is noteworthy that data mining uses a set of statistical and mathematical methods which can lead to recognition of the latent patterns and meaningful relationships within databases. Once a behavioral pattern has been identified among the databases and this pattern has been learned through mathematical and statistical models including regression, artificial neural networks, time series, etc., variations in the phenomenon behavior can be predicted, evaluated and interpreted based on its preceding behavior. Since the ARIMA model (Brockwell et al. 1991) involves a special set of univariate modeling for analysis and prediction of time series, the present study used the ARIMA (p, d and q) model to analyze time series of the calculated displacements for the epicenter of the earthquakes (as presented in Fig. 2b).

According to that, the measured data considered an anomaly when the difference between the predicted and actual values of the data goes beyond the range of RMSE defined by the statistical models; thus, the amount of crustal deformation anomalies of three months before the earthquake occurrence was calculated according to Eq. (1):

$$\text{Anamoly:} z_{\text{Real}} - z_{\text{calculated}} \mp \text{RMSE} \quad (1)$$

Identifying thermal anomalies at the epicenter of the earthquake

As already acknowledged by the previous researches, several phenomena are believed to trigger the increase in land surface temperature before the earthquake occurrence. Despite that the nature of this phenomenon and the mechanism of increasing land surface temperature before the earthquake are still vaguely understood (Qiang et al. 1997), monitoring thermal anomalies caused by earthquake can be one of the major approaches to estimate parameters related to earthquakes of magnitude larger than 4.5 on the Richter scale, which can be monitored by various thermal sensors and satellites in different spatial and temporal resolutions at TIR wavelengths (Tronin 2000; Huang et al. 2008).

Different studies have claimed different occurrence times of the LST anomalies with a wide range 1–24 days before the earthquake in the form of an increase in the temperature of 2–12 °C (Zhang et al. 2014; Pohn et al. 1974). It should be noted that in recent researches there are also other cases with a different range of 30–40 days before the earthquake that have been reported (Lu et al. 2016). On the other hand, considering the fact that the earth acts like an isothermal and homogenous surface during night and is exposed to thick clouds, shade, and direct sunlight during daytime, this could lead to the emergence of a temperature difference in the range of 15°–20° (Spencer et al. 1999), which would conceal thermal anomalies during the day. Thus, in the present study for providing reliable analysis of thermal anomalies and their relationship with earthquakes, average temperature day and night products were used. Also, considering that the temperature increase happens occasionally and locally along a fault, if there is no anomaly or turbulence within the area, all points (focal area and around it) will follow definite increasing or decreasing temperature patterns in each season. Therefore, it will be expectable that anomalies or turbulences such as the earthquake phenomenon may disrupt this compliance at the epicenter both spatially and temporally in comparison with other points within the area. So, in the present study as shown in Fig. 3b for calculating thermal anomalies unlike most of the previous investigations that have used time-series analysis methods to model temperature variations around the earthquake epicenter, the modeling of thermal variations was proposed taking into account the spatiotemporal correlations between epicenter thermal data and adjacent areas using regression functions Eq. (2). It should be noted that thermal anomalies detection

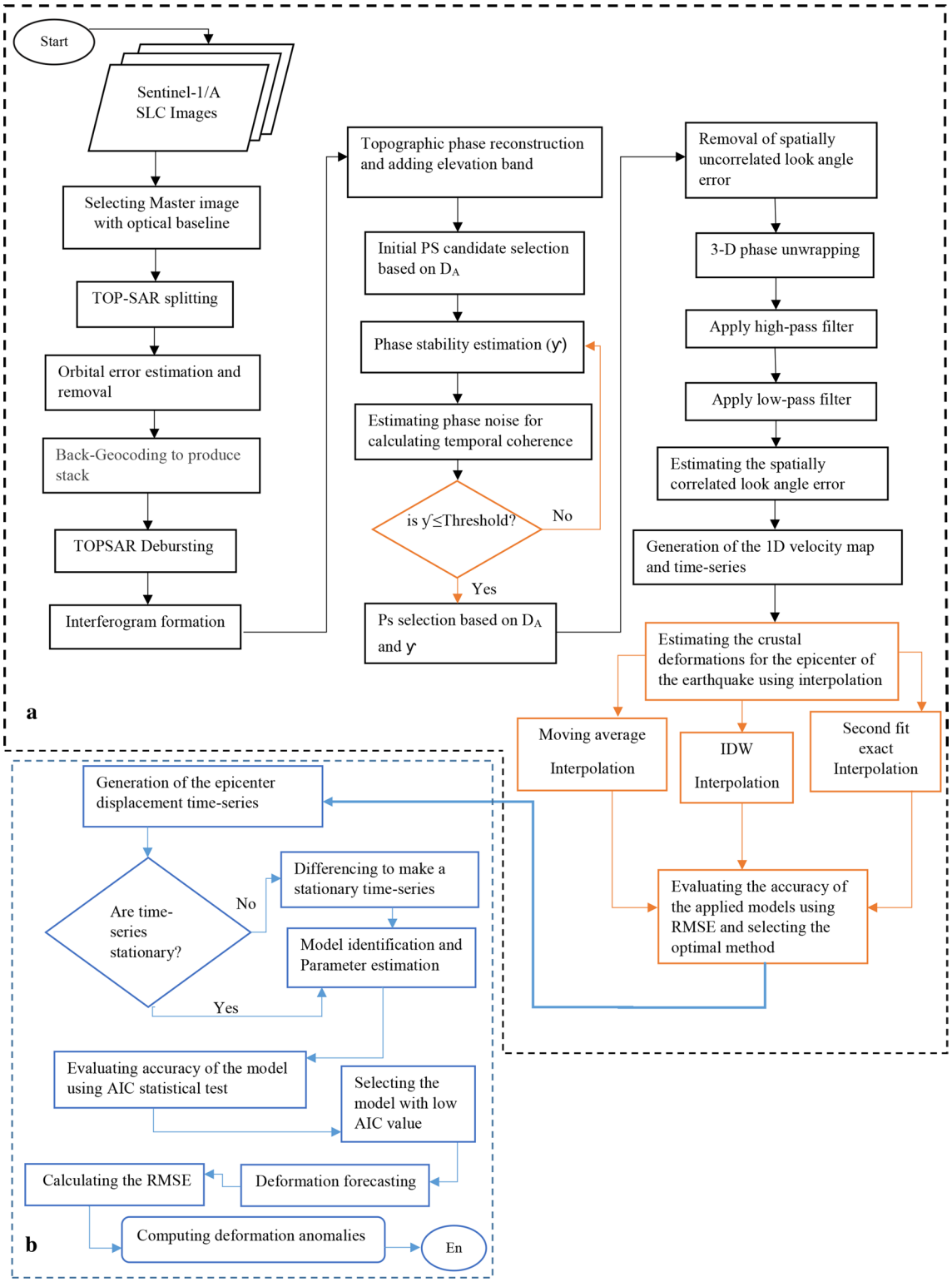

Fig. 2 Proposed algorithm for measuring surface displacement at the epicenter of the earthquake and calculating crustal deformation anomalies

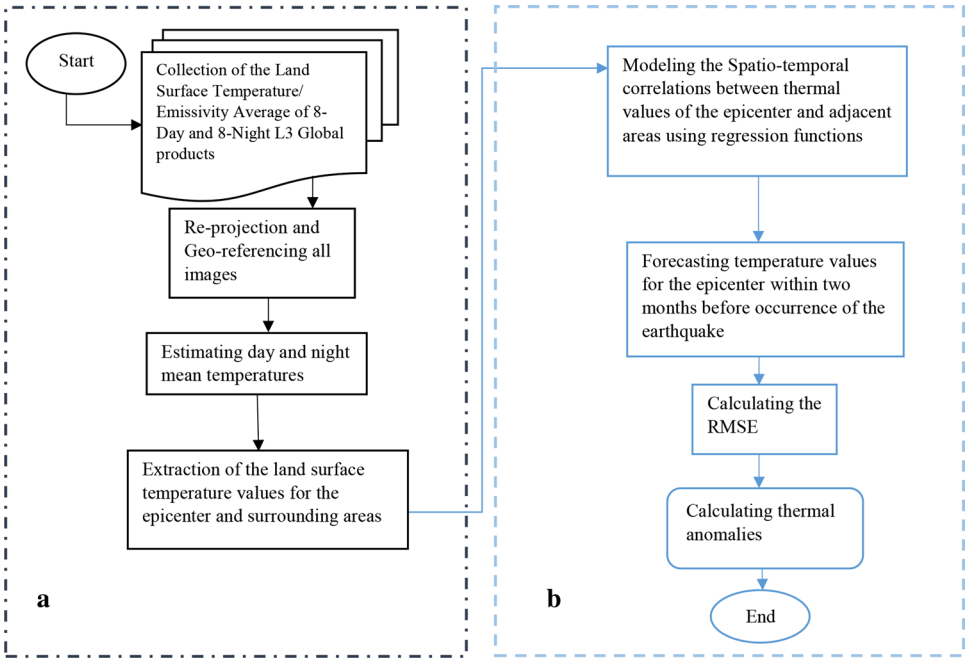

Fig. 3 Proposed algorithm for calculating thermal anomalies at the earthquake epicenter

through time series is merely based on temporal dependency among observation and without considering spatial dependency among them.

$$z(t) = a_0 + a_1 T_1 + a_2 T_2 + \cdots + a_p T_p \quad (2)$$

where a_0, a_1, …a_p are the model coefficients; T_1, T_2, ….T_p represent the temperature values related to each area; and $Z(t)$ represents the calculated temperature for time t.

Implementation

Properties of the study area

According to a large number of earthquakes with magnitude lower than 5.0 and considering that each of them can be considered as a foreshock for large magnitude earthquakes, predicting the occurrence of an earthquake of magnitude lower than 5.0 is not very valuable, both from a scientific and a practical point of view. On the other hand, considering that we implemented our proposed methods to monitor earthquake precursor anomalies on earthquakes with the same seismic properties and focal mechanism, to have an optimal distribution of sample regions, earthquakes with magnitude larger than 5.0 with nearly identical seismic properties from different regions of the world were selected. Table 1 presents the regional and seismic properties of each earthquake examined in the present study.

SOM results

As discussed in Sect. 2.1, in the present study thermal anomalies and crustal deformation anomalies have been monitored regarding the already happened earthquakes. But in this section results related to the implementation of the SOM algorithm to identify probable epicenters of the 2017 Kermanshah earthquake are presented (Figs. 4, 5).

Table 1 Properties of the earthquakes, extracted from the USGS Web site

Region	Focal geographic coordinates		Magnitude (Mw)	Depth (km)	Date	Time	Moment tensor
	Longitude	Latitude					
Iran, Kermanshah Province, 5 Km of Ezgeleh	45.90E	34.91N	7.3	19	2017/11/12	18:18:17(UTC)	Oblique thrust faulting
Mexico, 3km of San Pedro	97.97W	16.38N	7.2	22	2018/02/16	23:39:39(UTC)	Shallow-thrust faulting
Iran, Mashhad Province, 5 Km of Sefid Sang	60.43E	35.77N	6.1	13	2017/04/05	06:09:12(UTC)	Oblique thrust faulting
Iran, Bushehr Province, 4 Km of Kaki	51.61E	28.32N	5.5	10	2018/04/19	06:34:47(UTC)	Oblique thrust faulting

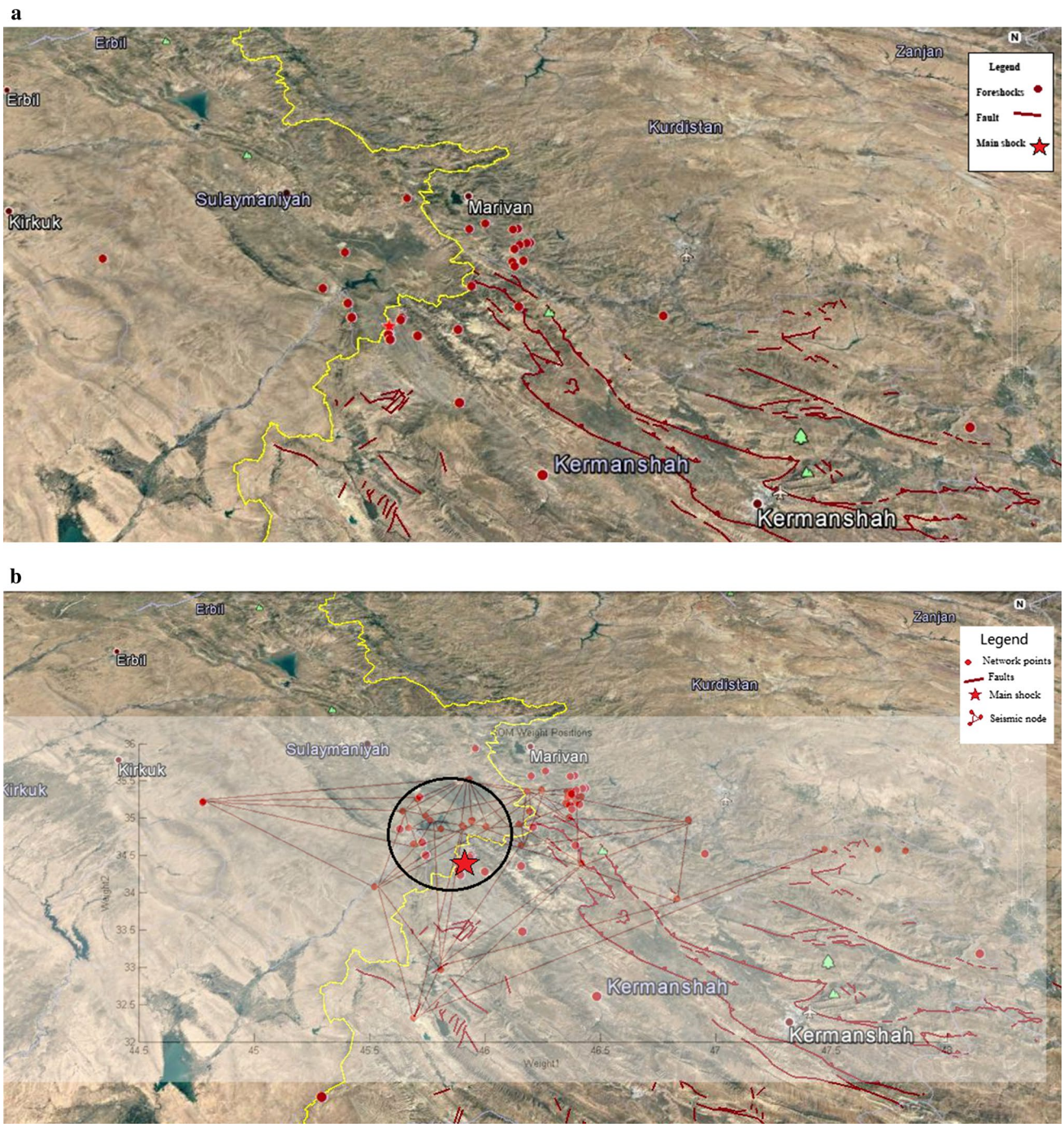

Fig. 4 **a** Topographic map of the Kermanshah Province. **b** Integration map of the SOM network output and topographic map of the Kermanshah Province

Determination of the crustal deformation anomalies at the earthquake epicenter

As discussed in Sect. 2.2, this study aimed at inspecting any significant relationship between crustal deformation anomalies at the epicenter of the earthquakes and probability of an earthquake through radar interferometry, so Sentinel-1 SAR data during a period of 14 months before each earthquake were used. Tables 2, 3, 4 and 5 present the properties of the SAR imagery used for this study.

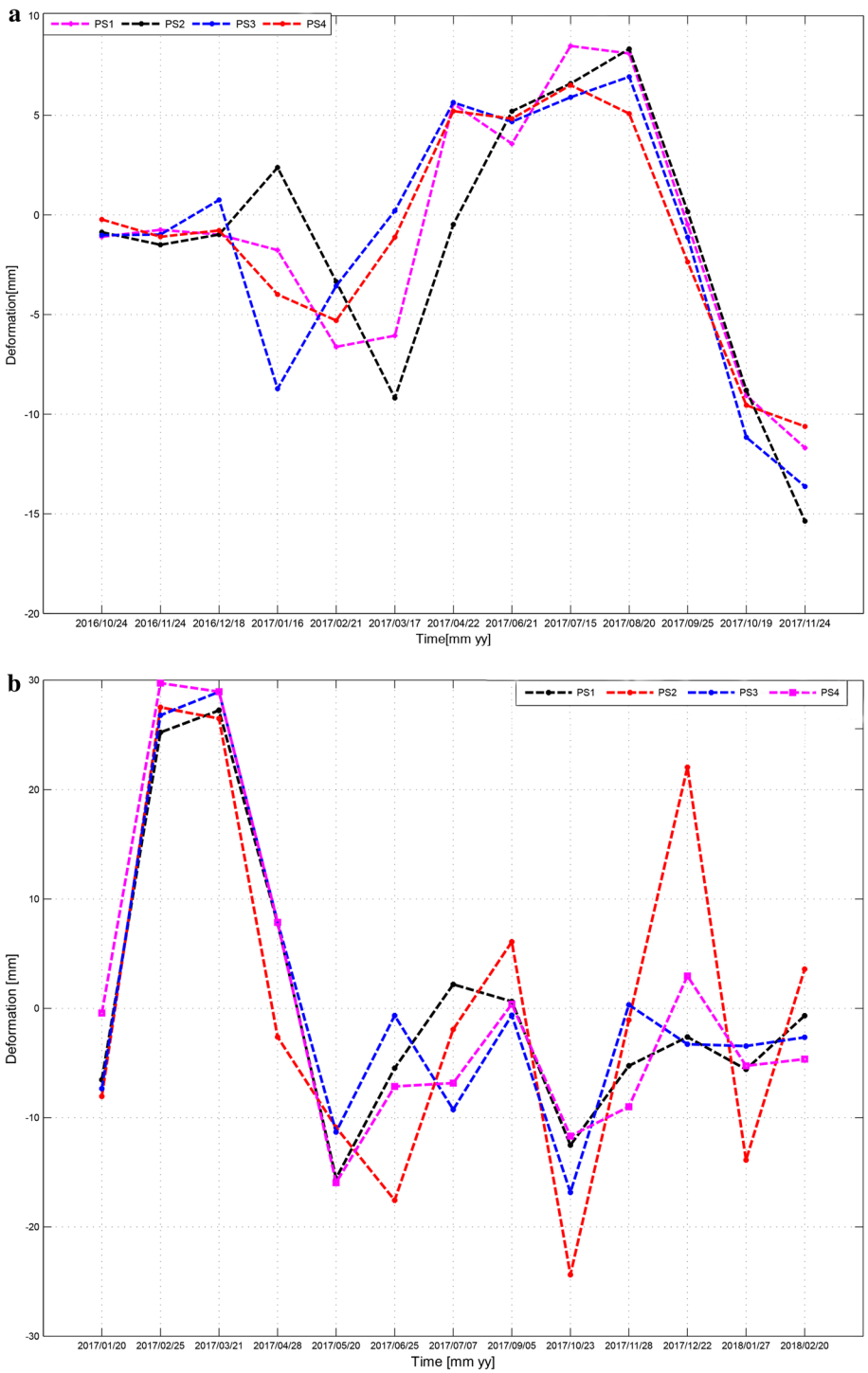

Fig. 5 **a** Time series of Line Of Sight (LOS) displacements for the selected PS points at the focal area of the Kermanshah Earthquake. **b** Time series of Line Of Sight (LOS) displacements for the selected PS points at the focal area of the Mexico Earthquake. **c** Time series of Line Of Sight (LOS) displacements for the selected PS points at the focal area of the Mashhad Earthquake. **d** Time series of Line Of Sight (LOS) displacements for the selected PS points at the focal area of the Bushehr Earthquake

Initial results of the extended-PS method

Final results of the extended-PS-InSAR

For the purposes of the present study aiming at estimating reliable values for the crustal deformations at the epicenter of the earthquakes based on the estimated displacements for PS points around the epicenter, three methods of interpolation were used including inverse distance weighted interpolation, moving average point interpolation and second fit exact interpolation. Then, for evaluating whether the accuracy of spatial sampling of the extended-PS method is adequate enough or not, obtained results from the above models were validated through RMSE statistical testing. By doing this, it will be possible to select the most accurate model so that surface deformations can be calculated for

Fig. 5 (continued)

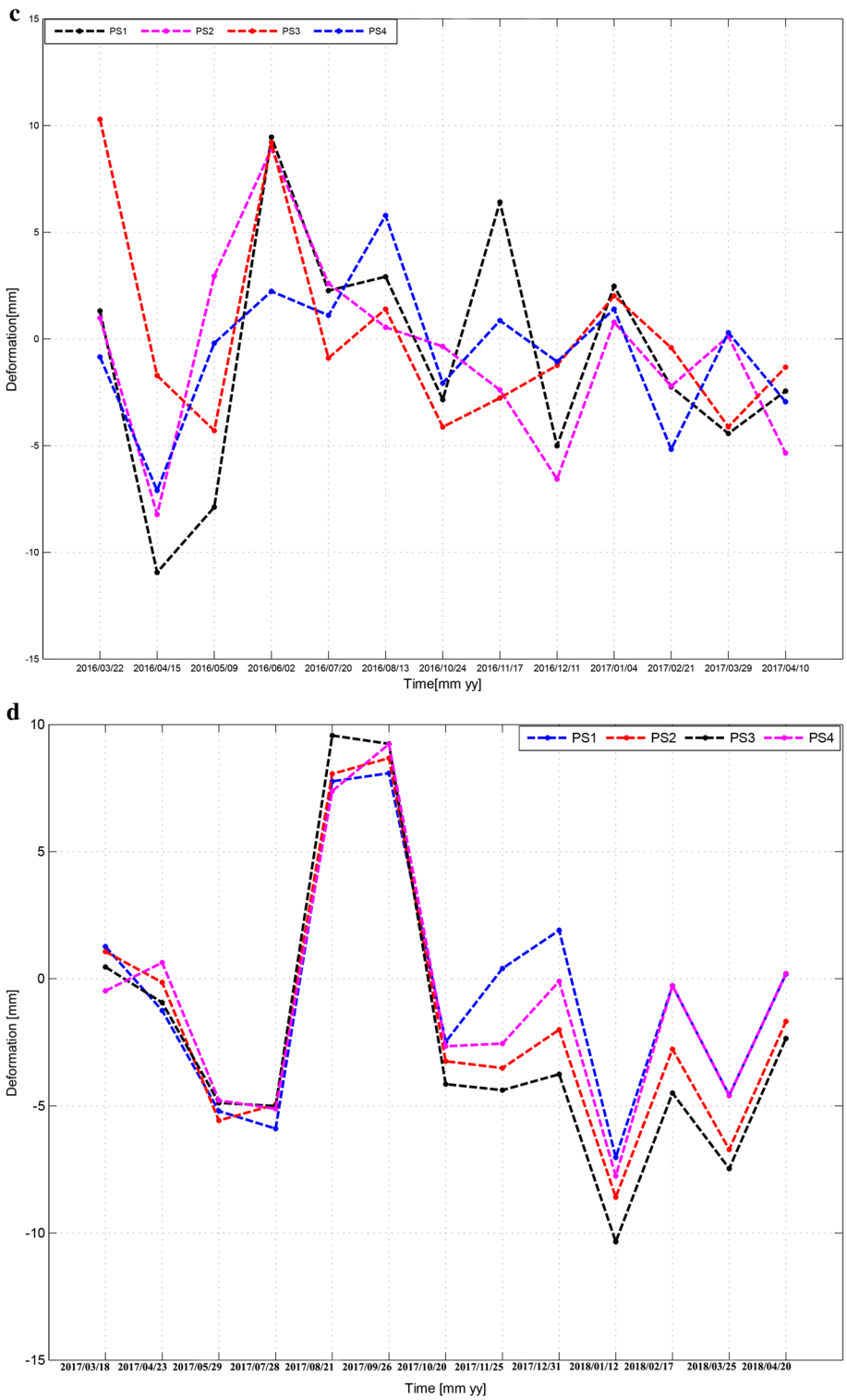

the epicenter of the earthquake. Table 6 presents the results of the accuracy of each method. By comparing all results, inverse distance weighting method was identified as the most desirable approach. Thus, it was used to extract land surface displacements at the epicenter of the earthquakes. Figure 6a–d illustrates these results.

Calculation of the crustal deformation anomalies using data mining approaches

As already described in Sect. 2.2.2, in order to perform behavioral analysis on epicenter deformation time series and calculate crustal deformation anomalies for earthquakes

Table 2 Properties of the SAR images used for Kermanshah region

Row	Satellite platform	Product type	Instrument mode	Time period	Orbit	Geometry
1	S1-A	SLC	IW	2016/10/24	13451	Descending
2	S1-A	SLC	IW	2016/11/24	14078	Descending
3	S1-A	SLC	IW	2016/12/18	14428	Descending
4	S1-A	SLC	IW	2017/01/16	14851	Descending
5	S1-A	SLC	IW	2017/02/21	15376	Descending
6	S1-A	SLC	IW	2017/03/17	15726	Descending
7	S1-A	SLC	IW	2017/04/22	16251	Descending
8	S1-A	SLC	IW	2017/05/16	16601	Descending
9	S1-A	SLC	IW	2017/06/21	17126	Descending
10	S1-A	SLC	IW	2017/07/15	17476	Descending
11	S1-A	SLC	IW	2017/08/20	18001	Descending
12	S1-A	SLC	IW	2017/09/25	18526	Descending
13	S1-A	SLC	IW	2017/10/19	18876	Descending
14	S1-A	SLC	IW	2017/11/24	19401	Descending

Table 3 Properties of the SAR images used for Mexico region

Row	Satellite platform	Product type	Instrument mode	Time period	Orbit	Geometry
1	S1-A	SLC	IW	2017/01/20	17190	Descending
2	S1-A	SLC	IW	2017/02/25	15440	Descending
3	S1-A	SLC	IW	2017/03/21	15790	Descending
4	S1-A	SLC	IW	2017/04/26	16315	Descending
5	S1-A	SLC	IW	2017/05/20	16665	Descending
6	S1-A	SLC	IW	2017/06/25	17190	Descending
7	S1-A	SLC	IW	2017/07/07	17365	Descending
8	S1-A	SLC	IW	2017/08/12	17890	Descending
9	S1-A	SLC	IW	2017/09/05	18240	Descending
10	S1-A	SLC	IW	2017/10/23	18940	Descending
11	S1-A	SLC	IW	2017/11/28	19465	Descending
12	S1-A	SLC	IW	2017/12/22	19815	Descending
13	S1-A	SLC	IW	2018/01/27	20340	Descending
14	S1-A	SLC	IW	2018/02/20	20690	Descending

epicenter, the ARIMA model with different orders of p and q was fitted to PS time series. Tables 7, 8, 9 and 10 present the modeling results, and Fig. 7a–d illustrates the crustal deformation anomalies for each region.

Estimation of the thermal anomalies at the epicenter of the earthquakes before the occurrence

For the purpose of finding out any significant relationship between behavioral variations of the thermal precursor and earthquake occurrence, considering the fact that maximum interval of this precursor has been reported in the range of 30–40 days before the earthquake, in this research, for each study area MODIS/Terra (MOD11A2) Land Surface Temperature/Emissivity average of 8-Day and 8-Night products were used for 2 months before the earthquake occurrence.

As already discussed in Sect. 2.3, in the present study, surface temperature variations at the epicenter were modeled based on temperatures of areas around the focal point using the proposed regression model (Eq. 2), during a period of 2 months before the earthquake. Finally, by comparing the estimated values of the model and the actual temperature available for the epicenter, thermal anomalies were calculated. Figure 8a–d illustrates the results of thermal anomalies.

Table 4 Properties of the SAR images used for Mashhad region

Row	Satellite platform	Product type	Instrument mode	Time period	Orbit	Geometry
1	S1-A	SLC	IW	2016/03/22	10483	Ascending
2	S1-A	SLC	IW	2016/04/15	10833	Ascending
3	S1-A	SLC	IW	2016/05/09	11183	Ascending
4	S1-A	SLC	IW	2016/06/02	11533	Ascending
5	S1-A	SLC	IW	2016/07/20	12233	Ascending
6	S1-A	SLC	IW	2016/08/13	12583	Ascending
7	S1-A	SLC	IW	2016/09/06	12933	Ascending
8	S1-A	SLC	IW	2016/10/24	13633	Ascending
9	S1-A	SLC	IW	2016/11/17	13983	Ascending
10	S1-A	SLC	IW	2016/12/11	14333	Ascending
11	S1-A	SLC	IW	2017/01/04	14683	Ascending
12	S1-A	SLC	IW	2017/02/21	15383	Ascending
13	S1-A	SLC	IW	2017/03/29	15908	Ascending
14	S1-A	SLC	IW	2017/04/10	16083	Ascending

Table 5 Properties of the SAR images used for Bushehr region

Row	Satellite platform	Product type	Instrument mode	Time period	Orbit	Geometry
1	S1-A	SLC	IW	2017/03/18	15748	Ascending
2	S1-A	SLC	IW	2017/04/23	16273	Ascending
3	S1-A	SLC	IW	2017/05/29	16798	Ascending
4	S1-A	SLC	IW	2017/06/22	17148	Ascending
5	S1-A	SLC	IW	2017/07/28	17673	Ascending
6	S1-A	SLC	IW	2017/08/21	18023	Ascending
7	S1-A	SLC	IW	2017/09/26	18548	Ascending
8	S1-A	SLC	IW	2017/10/20	18898	Ascending
9	S1-A	SLC	IW	2017/11/25	19423	Ascending
10	S1-A	SLC	IW	2017/12/31	19948	Ascending
11	S1-A	SLC	IW	2018/01/12	20123	Ascending
12	S1-A	SLC	IW	2018/02/17	20648	Ascending
13	S1-A	SLC	IW	2018/03/25	21173	Ascending
14	S1-A	SLC	IW	2018/04/20	21523	Ascending

Table 6 Accuracy of the applied interpolation methods for calculating crustal deformation at the epicenter of the earthquakes

Interpolation method	Modeling RMSE (mm) for Kermanshah earthquake	Modeling RMSE (mm) for Mexico earthquake	Modeling RMSE (mm) for Mashhad earthquake	Modeling RMSE (mm) for Bushehr earthquake
Linear second exact fit interpolation	±8.55 mm	±6.35 mm	±5.55 mm	±6.55 mm
Moving average interpolation	±4.58 mm	±3.28 mm	±4.53 mm	±2.58 mm
Inverse distance weighted interpolation	±1.69 mm	±1.23 mm	±1.75 mm	±0.69 mm

Discussion and Interpretation of the results

For the purposes of the present study, dealing with finding out a correlation between crustal deformation anomalies and thermal anomalies with an earthquake occurrence in the focal area is initially carried out in a unidimensional mode and then in an integrated form in order to offer a more reliable method to predict probable magnitude and

Table 7 Computational process of the crustal deformation anomalies of Kermanshah earthquake

Samples period	Monthly deformations (mm)	Stationary deformations (mm)	Fitted results (mm)	Residuals (mm)	Forecasted results (mm)
2016/10/24	−0.2	*	*	*	
2016/11/24	−3.0	−2.8	−0.14	−2.65	
2016/12/24	−4.9	−1.9	0.66	−2.55	
2017/01/24	−4.8	0.1	3.45	−3.35	
2017/02/24	−4.5	0.3	3.59	−3.29	
2017/03/24	4.1	8.6	4.07	4.52	
2017/04/24	5.1	1.0	2.07	−1.07	
2017/05/24	5.1	0.0	−1.41	1.41	
2017/06/24	7.1	2.0	1.46	0.53	
2017/07/24	7.5	0.4	0.12	0.27	
2017/08/24	6.1	−1.4	0.74	−2.14	
2017/09/24	0.7				1.51
2017/10/24	−7.5				2.49
2017/11/24	−12.5				1.14

Table 8 Computational process of the crustal deformation anomalies of Mexico earthquake

Samples' period	Monthly deformations (mm)	Stationary deformations (mm)	Fitted results (mm)	Residuals (mm)	Forecasted results (mm)
2017/01/20	−7.30	*	*	*	
2017/02/20	22.12	29.42	30.13	−0.71	
2017/03/20	27.00	4.88	8.37	−3.49	
2017/04/20	6.83	−20.17	−25.48	5.31	
2017/05/20	−14.38	−21.21	−22.79	1.58	
2017/06/20	−10.38	4.00	2.48	1.51	
2017/07/20	−2.35	8.03	20.65	−12.62	
2017/08/20	1.39	3.74	7.60	−3.86	
2017/09/20	−3.10	−4.49	−2.67	−1.81	
2017/10/20	−14.80	−11.70	−6.61	−5.08	
2017/11/20	−6.25	8.55	−1.28	9.83	
2017/12/20	9.38				9.73
2018/01/20	−15.3				−5.61
2018/02/20	1.39				−15.17

time of earthquake occurrence anomalies within earthquake-prone regions.

Interpretation of the detected crustal deformation anomalies

Figure 7a shows the crustal deformation anomalies of Kermanshah earthquake; the behavior of the anomalous structure shows that after observation subsidence within 3 months before the earthquake and by increasing the rate of this subsidence in the future months, an earthquake of magnitude of 7.3 occurs during a period of 19 days after observing the first subsidence. Behavioral analysis is performed on crustal deformation anomalies related to another earthquake of magnitude of 7.2 and similar focal mechanism. As shown in Fig. 7b, the crustal deformation anomalies at the epicenter of the Mexico earthquake follow a half cycle of the sinusoidal waveform before the earthquake. For the earthquakes with magnitude of lower than 7.0 and larger than 5.0, as shown by crustal deformation anomalies of Mashhad earthquake (Fig. 7c), the behavior of the anomalous structure has been viewed as subsidence for 2 months before the earthquakes. while the behavioral variations of the crustal deformation anomalies of an earthquake with similar seismic properties, as shown in diagram d (Fig. 7), shows a different pattern of subsidence at the epicenter before the

Table 9 Computational process of the crustal deformation anomalies of Mashhad earthquake

Samples' period	Monthly deformations (mm)	Stationary deformations (mm)	Fitted results (mm)	Residuals (mm)	Forecasted results (mm)
2016/03/22	2.93	*	*	*	
2016/04/22	−5.78	−8.71	−3.89	−4.81	
2016/05/22	1.1	6.88	3.86	3.01	
2016/06/22	7.1	6.00	4.61	1.38	
2016/07/22	1.1	−6.00	−5.51	−0.48	
2016/08/22	1.2	0.10	−1.72	1.82	
2016/09/22	−0.82	−2.02	−0.75	−1.26	
2016/10/22	−2.1	−1.28	−1.75	0.47	
2016/11/22	−0.54	1.56	1.38	0.17	
2016/12/22	−2.9	−2.36	−0.90	−1.45	
2017/01/22	0.10	3.00	0.77	2.22	
2017/02/22	−2.20				0.34
2017/03/22	−2.60				−3.30
2017/04/22	−2.40				−0.07

Table 10 Computational process of the crustal deformation anomalies of Bushehr earthquake

Samples period	Monthly deformations (mm)	Stationary deformations (mm)	Fitted results (mm)	Residuals (mm)	Forecasted results (mm)
2017/03/18	0.36	*	*	*	
2017/04/18	−0.62	−0.98	1.30	−2.28	
2017/05/18	−4.22	−3.60	−0.63	−2.96	
2017/06/18	−5.01	−0.79	3.07	−3.86	
2017/07/18	−5.01	0.00	4.48	−4.48	
2017/08/18	8.50	13.51	6.05	7.45	
2017/09/18	8.90	0.40	0.70	−0.30	
2017/10/18	−3.61	−12.51	−11.80	−0.70	
2017/11/18	−3.90	−0.29	−0.84	0.55	
2017/12/18	−2.78	1.12	−0.94	2.06	
2018/01/18	−8.30	−5.52	−3.47	−2.04	
2018/02/18	−3.22				−3.42
2018/03/18	−6.10				1.20
2018/04/18	−2.40				−1.63

earthquake. Considering that the amounts of crustal deformation anomalies and their behaviors are different in earthquakes with a magnitude of larger than or equal to 7.0 as well as earthquakes with a magnitude of lower than or 7.0, we cannot deduce a general index for predicting the probable magnitude or time of earthquake occurrence.

Interpretation of the detected thermal anomalies

In the case of interpretation of the thermal anomalies at the epicenter of the earthquakes, unlike previous works in this field, the present study by modeling spatiotemporal dependence of thermal variations using regression functions proved that earthquake prediction based on the thermal anomalies will be unreliable by identifying the positive thermal anomalies and correlating them with the main fault of the earthquake merely, because the thermal anomalies before the earthquake may also have a negative values. In other words, an unusual increase or decrease in temperature variations of the probable epicenter can be considered as a thermal anomaly.

In the case of behavioral analysis on thermal anomalies, as shown in Fig. 8a, b, it is not possible to detect a consistent and constant pattern related to earthquake occurrence with a magnitude of 7.0 or higher because of irregularities seen in the behavior of thermal anomalies two months before the

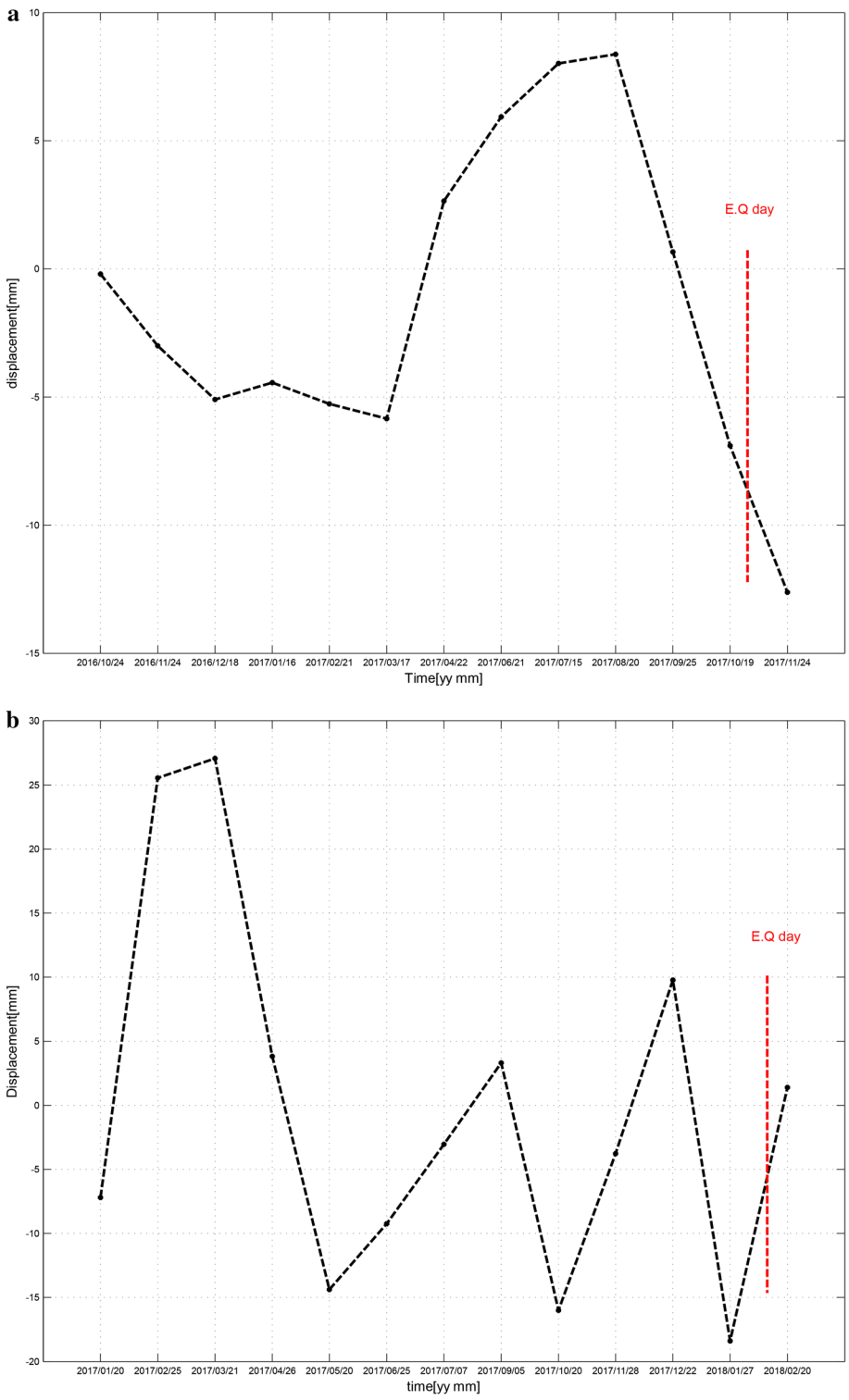

Fig. 6 **a** Time series of line-of-sight (LOS) displacements at the epicenter of Kermanshah earthquake with the accuracy of ± 1.69 mm. **b** Time series of line-of-sight (LOS) displacements at the epicenter of Mexico earthquake with the accuracy of ± 1.23 mm. **c**: Time series of line-of-sight (LOS) displacements at the epicenter of Mashhad earthquake with the accuracy of ± 1.75 mm. **d** Time series of line-of-sight (LOS) displacements at the epicenter of Bushehr earthquake with the accuracy of ± 0.69 mm

earthquake. Moreover, frequent irregularities in the variation rate of thermal anomalies estimated for earthquakes with a magnitude of lower than 7.0 and larger than 5.0 (Fig. 8c, d), prevent identification of the significant correlation between focal thermal anomalies and occurrence of an earthquake.

Integrated interpretation of detected thermal anomalies and crustal deformation anomalies at the epicenter of the earthquake

However, the absence of any significant correlation between calculated thermal and crustal deformation

Fig. 6 (continued)

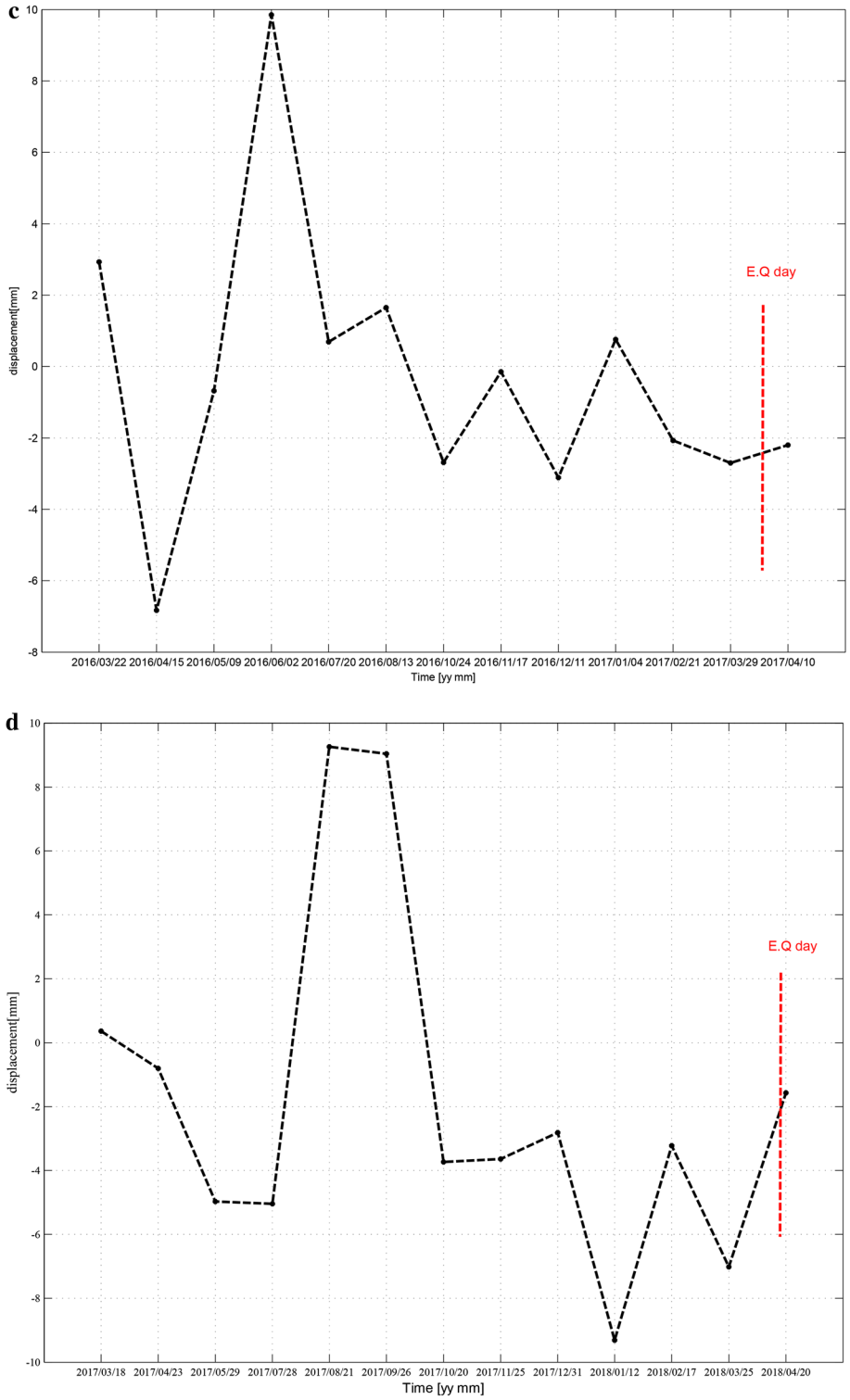

anomalies and earthquakes, in unidimensional mode, never underestimates precursors and estimated anomalies for each precursor. On the other hand, in the research process, after the extraction of crustal deformation anomalies and thermal anomalies before the earthquake occurrence, the temporal correlation analyzing between these two data sets was analyzed. The results of the analyses showed that there is no one-to-one temporal correspondence between these two data sets, and the relationship between them is only related to the maximum amount of the anomalies. Accordingly, the use of spatiotemporal models was not effective. Therefore, in the present study, instead of

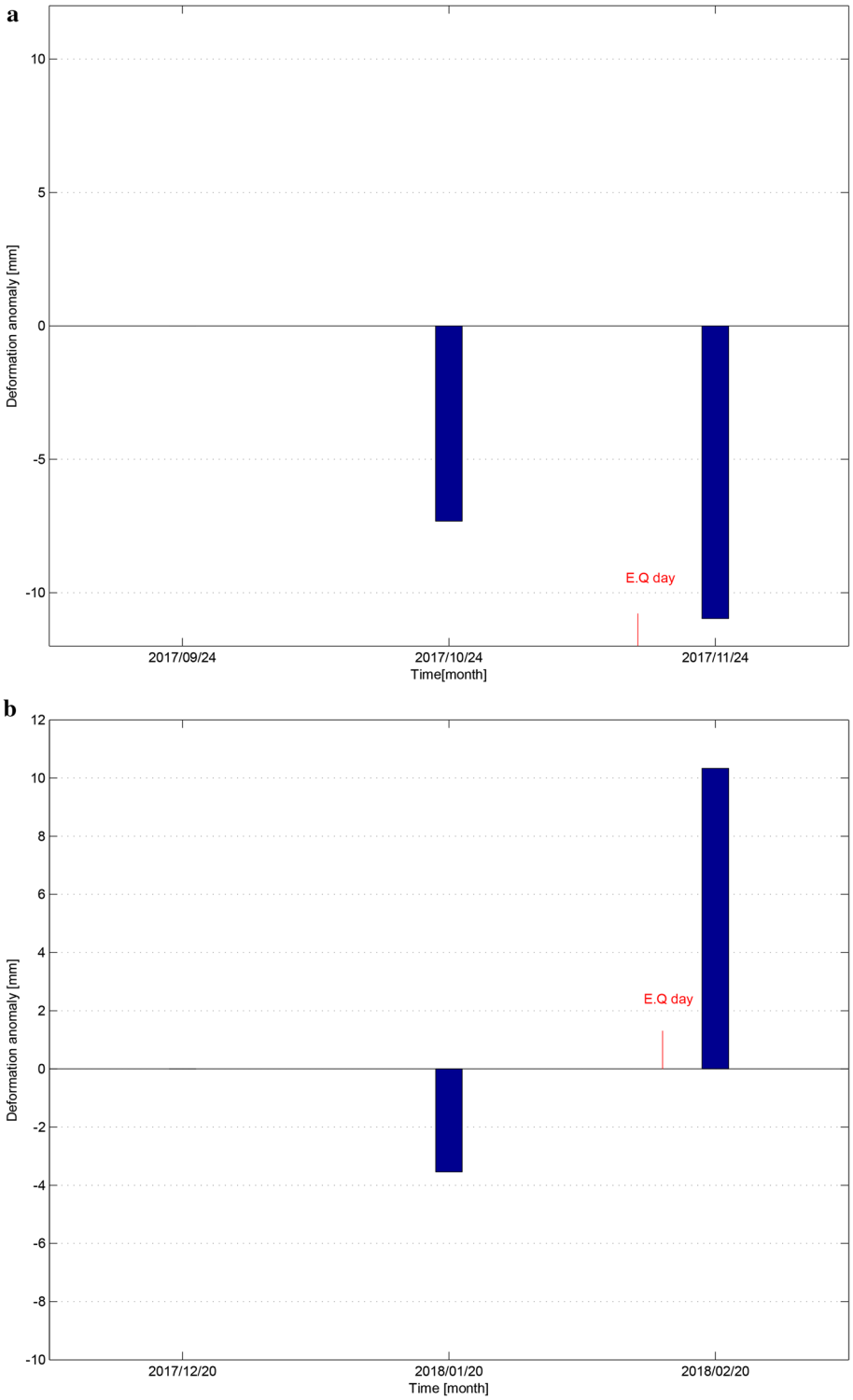

Fig. 7 **a** Crustal deformation anomalies at the epicenter of Kermanshah earthquake within 3 months before the occurrence. **b**: Crustal deformation anomalies at the epicenter of Mexico earthquake within 3 months before the occurrence. **c** Crustal deformation anomalies at the epicenter of Mashhad earthquake within 3 months before the occurrence. **d** Crustal deformation anomalies at the epicenter of Bushehr earthquake within 3 months before the occurrence

examining general and unidimensional behavior of the detected anomalies, maximum crustal deformation anomaly and maximum thermal anomaly at the earthquake's epicenter in a period of two months before earthquake based on their value and interval from the day of the event were extracted (as shown in Table 11). Then, a descriptive and logical rule as earthquake prediction algorithm based on amount and time of observing maximum crustal deformation anomaly and the maximum thermal anomaly of earthquakes with oblique thrust faulting was proposed (as shown in Fig. 9).

Fig. 7 (continued)

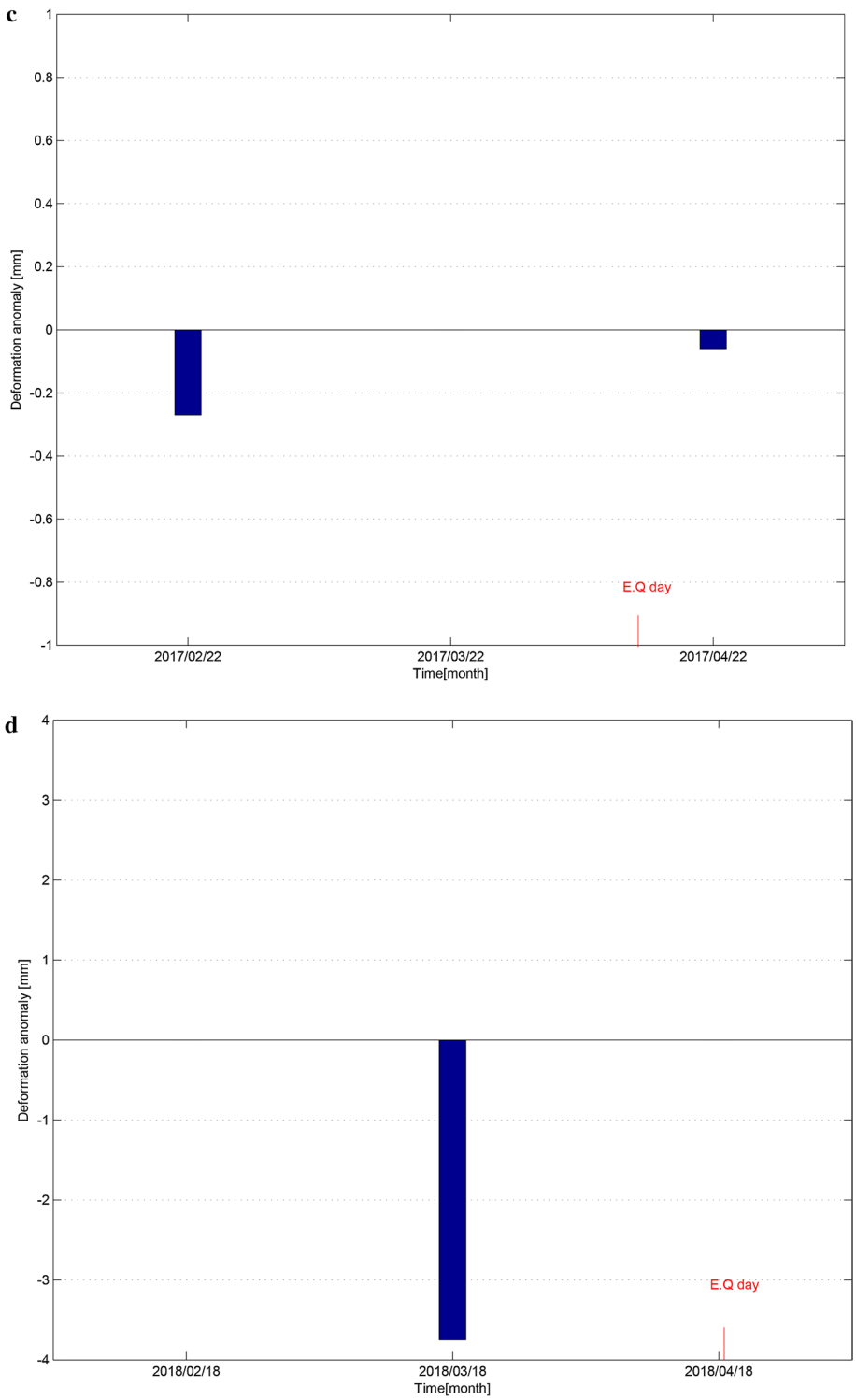

Evaluation of the efficiency of the proposed earthquake prediction algorithm for an earthquake with a different focal mechanism

In this section, the efficiency of the proposed algorithm in Sect. 4.3 was evaluated for an earthquake with a different focal mechanism. We selected April 16, 2016, Japan-Kumamoto earthquake of magnitude 7.0 with strike-slip faulting for performing this test. Figure 10a–c illustrates the results.

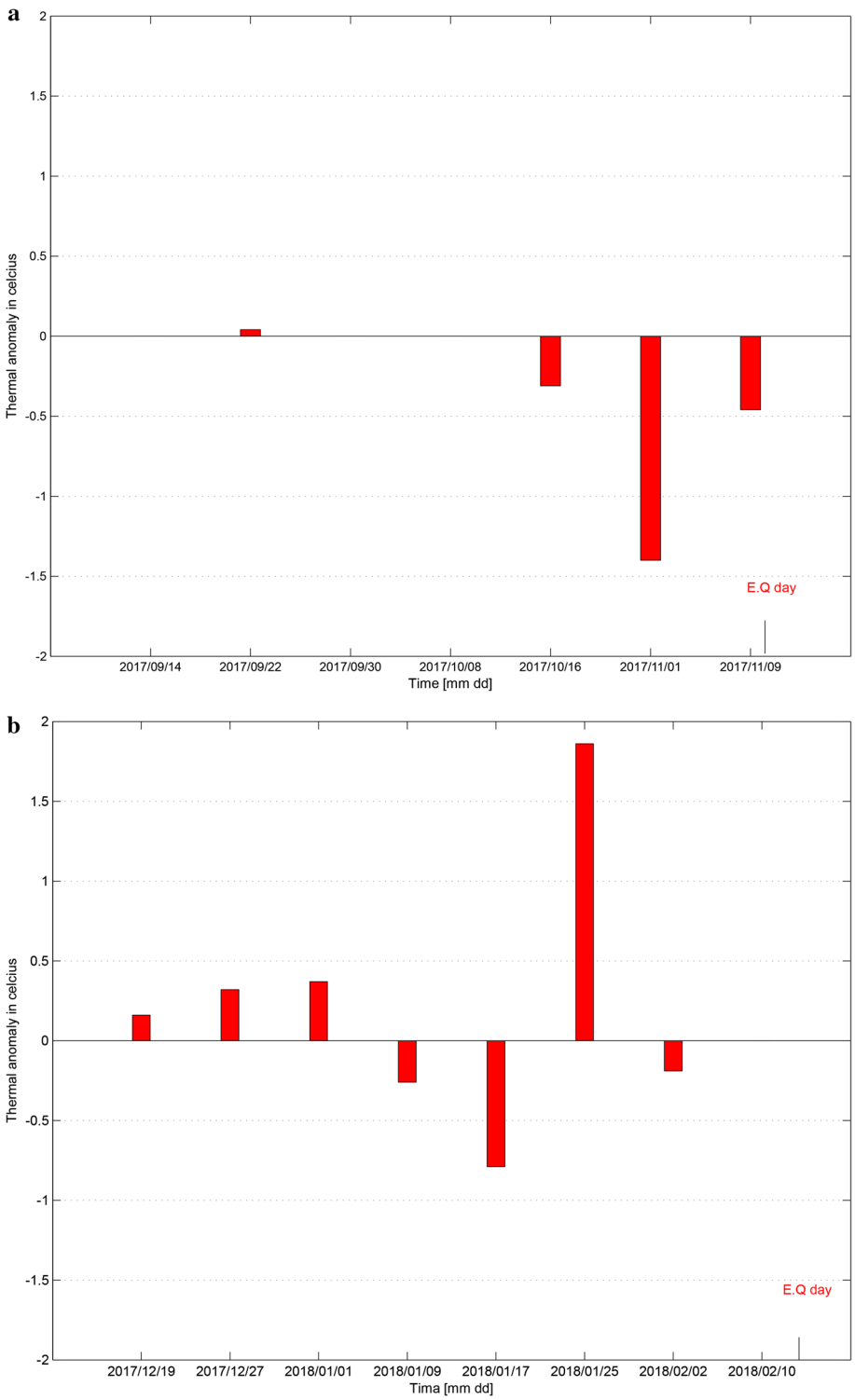

Fig. 8 **a** Thermal anomalies during a period of 2 months at the epicenter of Kermanshah earthquake. **b** Thermal anomalies during a period of 2 months at the epicenter of Mexico earthquake. **c** Thermal anomalies during a period of 2 months at the epicenter of Mashhad earthquake. **d** Thermal anomalies during a period of 2 months at the epicenter of Bushehr earthquake

Conclusion

According to the obtained results from this study, thermal anomalies and crustal deformation anomalies at the epicenter of earthquakes with similar focal mechanism and similar seismic characteristics show different structural patterns before earthquake occurrence. Therefore, making deterministic earthquake prediction based on individual monitoring of thermal anomalies in the focal area, as well as monitoring of the crustal deformation anomalies, is practically impossible. Also, during the research process, separate time series and regression analyses were

Fig. 8 (continued)

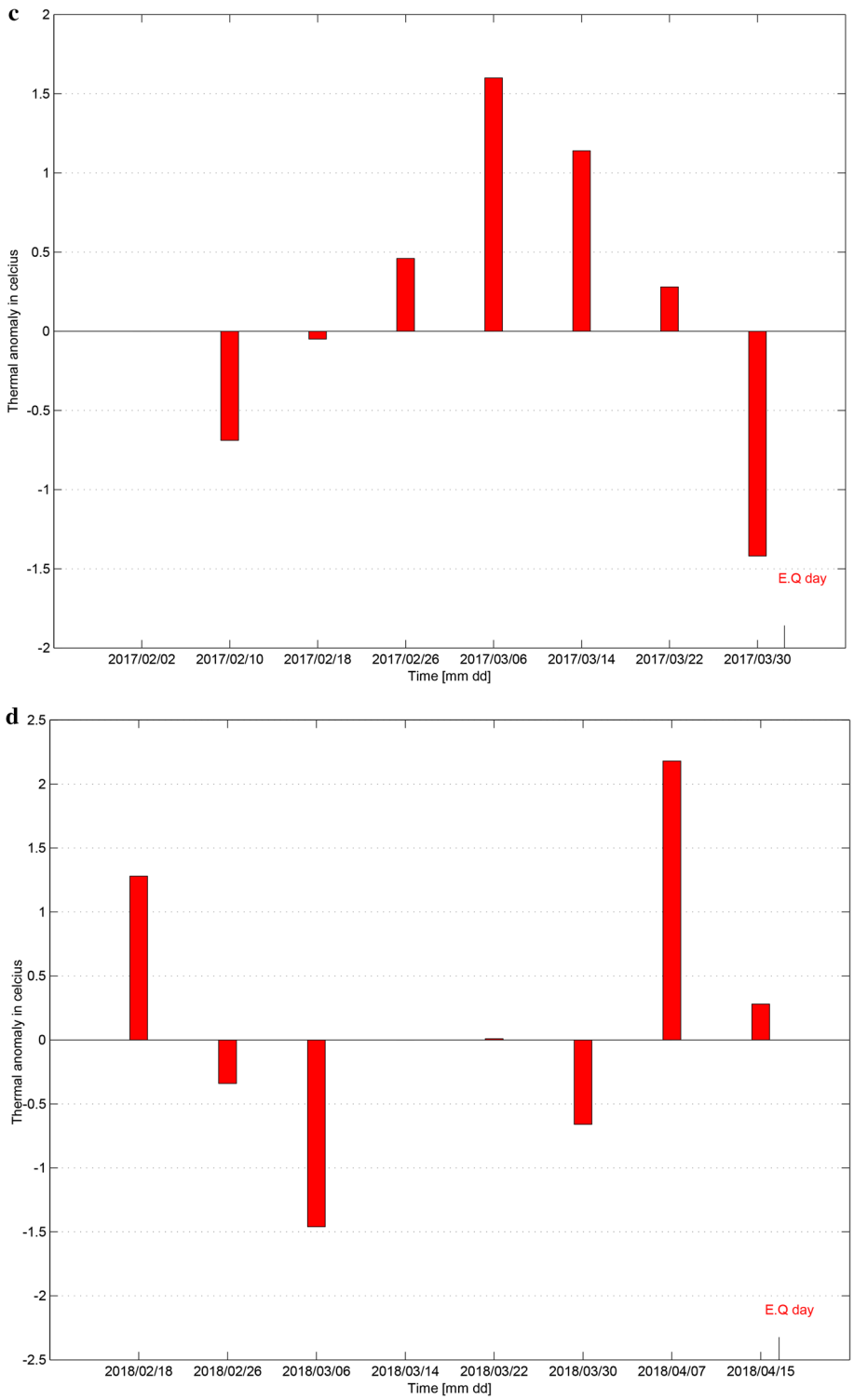

carried out on the extracted thermal anomalies and crustal deformation anomalies. Unfortunately, none of the above-mentioned methods resulted in a deterministic index for the prediction of an earthquake occurrence. Despite the fact that the existence of different structures in the crustal deformation anomalies and thermal anomalies in the focal area prevented modeling unidimensional correlation between these precursors with earthquake occurrence, in this study, by considering the maximum amount of thermal anomalies and crustal deformation anomalies in a period of 2 months before earthquake occurrence, a descriptive and logical rule as an earthquake prediction algorithm in

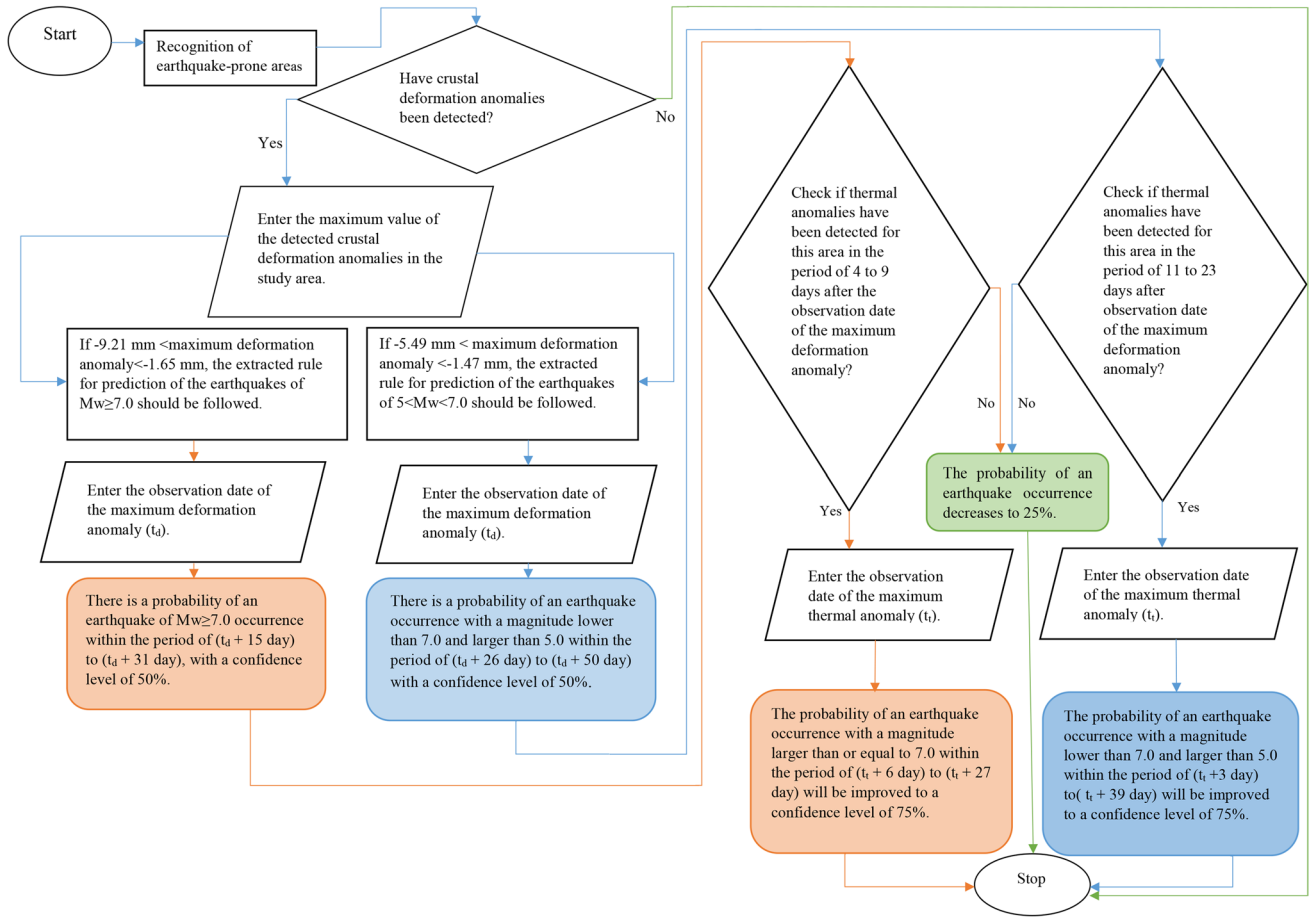

Fig. 9 Proposed algorithm to investigate the probability of an earthquake occurrence based on observing maximum anomalies of crustal deformation and surface temperature of earthquakes with oblique thrust faulting

Table 11 Maximum amounts of thermal anomalies and crustal deformation anomalies at the epicenter of the earthquakes within two months before the earthquake

Region	Maximum value of the crustal deformation anomaly within 2 months before the earthquake occurrence (mm)	Time interval between the maximum crustal deformation anomaly and the earthquake day (day)	Maximum value of the thermal anomaly within 2 months before the earthquake occurrence (c°)	Time interval between the maximum thermal anomaly and the earthquake day (day)
Iran, Kermanshah Province, 5 km of Ezgeleh	− 7.32	19	− 1.40	11
Mexico, 3 km of San Pedro	− 3.54	27	+ 1.86	22
Iran, Mashhad Province, 5 km of Sefid Sang	− 0.27	44	+ 1.61	30
Iran, Bushehr Province, 4 km of Kaki	− 3.75	32	+ 2.18	12

the case of earthquakes with oblique thrust faulting was proposed (see Fig. 9). Since the investigated earthquakes for the purposes of this study were oblique thrust earthquakes, the validity of the proposed algorithm was evaluated for an earthquake with a different focal mechanism. The analysis results of the thermal anomalies and crustal deformation anomalies at the epicenter of April 16, 2016, Japan-Kumamoto earthquake of magnitude 7.0 with strike-slip faulting, showed completely different trends than the suggested patterns by the proposed algorithm. So the

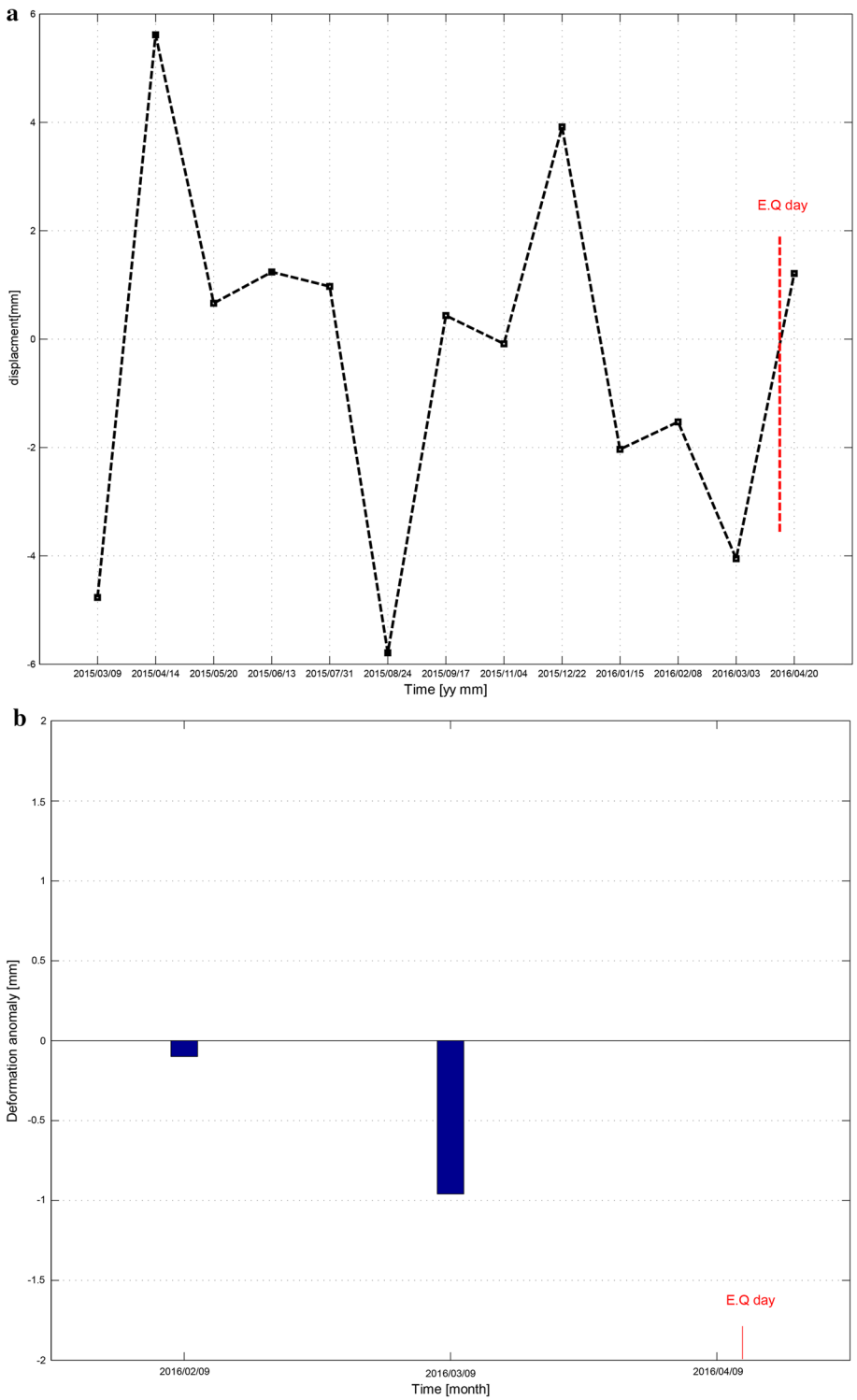

Fig. 10 **a** Time series of line-of-sight (LOS) displacements at the epicenter of Japan-Kumamoto earthquake with the accuracy of ± 1.23 mm. **b** Crustal deformation anomalies at the epicenter of Japan-Kumamoto earthquake within 3 months before the earthquake. **c** Thermal anomalies during a period of 2 months at the epicenter of Japan-Kumamoto earthquake

proposed algorithm was unable to determine the probable time and magnitude of an earthquake occurrence with strike-slip faulting. Therefore, it is recommended that, in order to complete the proposed prediction algorithm by this study, its performance must be tested with more study samples.

Fig. 10 (continued)

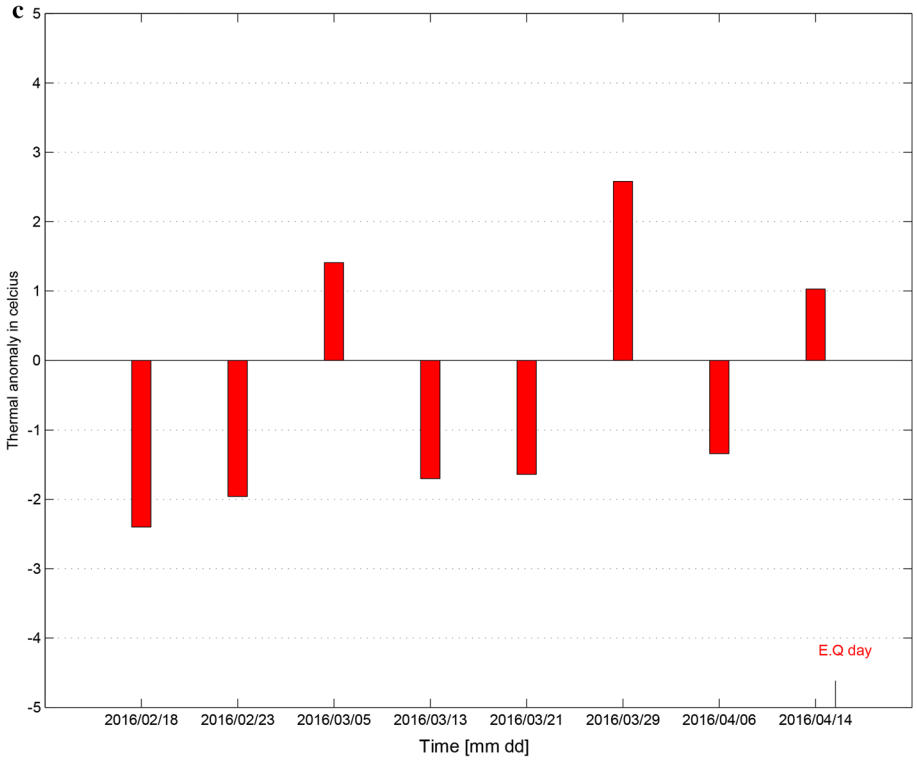

References

Akhoondzadeh M, Parrot M, Saradjian M (2010) Electron and ion density variations before strong earthquakes (M%3e 6.0) using DEMETER and GPS data. Nat Hazards Earth Syst Sci 10:7–18

Bamler R, Hartl P (1998) Synthetic aperture radar interferometry. Inverse Prob 14(4):R1

Brockwell PJ, Davis RA, Fienberg SE (1991) Time-series: theory and methods. Springer, Berlin

Bürgmann R, Rosen PA, Fielding EJ (2000) Synthetic aperture radar interferometry to measure Earth's surface topography and its deformation. Annu Rev Earth Planet Sci 28(1):169–209

Calais E, Vergnolle M, San'Kov V et al (2003) GPS measurements of crustal deformation in the Baikal-Mongolia area (1994–2002): implications for current kinematics of Asia. J Geophys Res Solid Earth 108:2501

Gabriel AK, Goldstein RM, Zebker HA (1989) Mapping small elevation changes over large areas: differential radar interferometry. J Geophys Res Solid Earth 94(B7):9183–9191

Graham LC (1974) Synthetic interferometer radar for topographic mapping. Proc IEEE 62(6):763–768

Grant RA, Raulin JP, Freund FT (2015) Changes in animal activity prior to a major (M= 7) earthquake in the Peruvian Andes. Phys Chem Earth Parts A/B/C 85:69–77

Guo G, Wang B (2008) Cloud anomaly before Iran earthquake. Int J Remote Sens 29:1921–1928

Han P, Hattori K, Huang Q et al (2011) Evaluation of ULF electromagnetic phenomena associated with the 2000 Izu Islands earthquake swarm by wavelet transform analysis. Nat Hazards Earth Syst Sci 11:965–970

Hand DJ (2007) Principles of data mining. Drug Saf 30:621–622

Hayakawa M (2013) Possible electromagnetic effects on abnormal animal behavior before an earthquake. Animals 3:19–32

Hooper A (2008) A multi-temporal InSAR method incorporating both persistent scatterer and small baseline approaches. Geophys Res Lett 35(16):16302

Huang J, Mao F, Zhou W, Zhu X (2008) Satellite thermal IR associated with Wenchuan earthquake in China using MODIS data. In: Paper presented at the proceeding of the 14th world conference on earthquake engineering.

Huang F, Li M, Ma Y et al (2017) Studies on earthquake precursors in China: a review for recent 50 years. Geod Geodyn 8:1–12

Ingebritsen SE, Manga M (2014) Earthquakes: hydrogeochemical precursors. Nat Geosci 7:697

Li J, Heap AD (2014) Spatial interpolation methods applied in the environmental sciences: a review. Environ Modell Softw 53:173–189

Lippiello E, Marzocchi W, de Arcangelis L, Godano C (2012) Spatial organization of foreshocks as a tool to forecast large earthquakes. Sci Rep 2:846

Lu X, Meng Q, Gu X et al (2016) Thermal infrared anomalies associated with multi-year earthquakes in the Tibet region based on China's FY-2E satellite data. Adv Space Res 58:989–1001

Massonnet D, Feigl KL (1998) Radar interferometry and its application to changes in the Earth's surface. Rev Geophys 36:441–500

Massonnet D, Rossi M, Carmona C, Adragna F, Peltzer G, Feigl K, Rabaute T (1993) The displacement field of the Landers earthquake mapped by radar interferometry. Nature 364(6433):138

Mohankumar K, Sangeetha K (2018) A study on earthquake prediction using neural network algorithms

Molchanov O, Rozhnoi A, Solovieva M et al (2006) Global diagnostics of the ionospheric perturbations related to the seismic activity using the VLF radio signals collected on the DEMETER satellite. Nat Hazards Earth Syst Sci 6:745–753

Moreno M, Rosenau M, Oncken O (2010) 2010 Maule earthquake slip correlates with pre-seismic locking of Andean subduction zone. Nature 467:198

Moro M, Saroli M, Stramondo S et al (2017) New insights into earthquake precursors from InSAR. Sci Rep 7:12035

Ogata Y, Katsura K (2012) Prospective foreshock forecast experiment during the last 17 years. Geophys J Int 191:1237–1244

Parsons, B. (2017) From geodesy to tectonics: observing earthquake processes from space (Augustus Love Medal Lecture). In: Paper presented at the EGU general assembly conference abstracts.

Peacock S, Crampin S, Booth DC, Fletcher JB (1988) Shear wave splitting in the Anza seismic gap, southern California: temporal variations as possible precursors. J Geophys Res Solid Earth 93:3339–3356

Peltzer G, Rosen P (1995) Surface displacement of the 17 May 1993 Eureka Valley, California, earthquake observed by SAR interferometry. Science 268(5215):1333–1336

Pio Lucente F, De Gori P, Margheriti L et al (2010) Temporal variation of seismic velocity and anisotropy before the 2009 MW 6.3 L'Aquila earthquake Italy. Geology 38:1015–1018

Pohn H, Offield T, Watson K (1974) Thermal inertia mapping from satellite-discrimination of geologic units in Oman. J Res US Geol Surv 2:147–158

Pulinets S, Davidenko D (2014) Ionospheric precursors of earthquakes and global electric circuit. Adv Space Res 53:709–723

Pulinets S, Ouzounov D, Karelin A, Boyarchuk K, Pokhmelnykh L (2006) The physical nature of thermal anomalies observed before strong earthquakes. Phys Chem Earth Parts A/B/C 31:143–153

Qiang Z-J, Kong L-C, Zheng L-Z et al (1997) An experimental study on temperature increasing mechanism of satellitic thermo-infrared. Acta Seismol Sin 10:247–252

Rikitake T (1968) Earthquake prediction. Earth Sci Rev 4:245–282

Rikitake T (1975) Earthquake precursors. Bull Seismol Soc Am 65:1133–1162

Rosen PA, Hensley S, Joughin IR, Li F, Madsen SN, Rodriguez E, Goldstein RM (1998) Synthetic aperture radar interferometry. Proceed IEEE 88(3):333–382

Saradjian M, Akhoondzadeh M (2011) Thermal anomalies detection before strong earthquakes (M%3e 6.0) using interquartile, wavelet and Kalman filter methods. Nat Hazards Earth Syst Sci 11:1099–1108

Saraf AK, Rawat V, Choudhury S, Dasgupta S, Das J (2009) Advances in understanding of the mechanism for generation of earthquake thermal precursors detected by satellites. Int J Appl Earth Obs Geoinf 11:373–379

Spencer JR, Tamppari LK, Martin TZ, Travis LD (1999) Temperatures on Europa from Galileo photopolarimeter-radiometer: nighttime thermal anomalies. Science 284(5419):1514–1516

Thomas D (1988) Geochemical precursors to seismic activity. Pure Appl Geophys 126:241–266

Thomas J, Masci F, Love JJ (2015) On a report that the 2012 M6: 0 earthquake in Italy was predicted after seeing an unusual cloud formation. Nat Hazards Earth Syst Sci 15:1061–1068

Tomás R, Romero R, Mulas J et al (2014) Radar interferometry techniques for the study of ground subsidence phenomena: a review of practical issues through cases in Spain. Environ Earth Sci 71:163–181

Tronin A (2000) Thermal IR satellite sensor data application for earthquake research in China. Int J Remote Sens 21(16):3169–3177

Tsai C-H, Chen C-W (2010) An earthquake disaster management mechanism based on risk assessment information for the tourism industry-a case study from the island of Taiwan. Tour Manag 31:470–481

Tu PF, Xia L, Li HT, Wu SC (2012) PSInSAR technology research and its application on landslide monitoring. In: Paper presented at the applied mechanics and materials

Wang T, Zhuang J, Kato T, Bebbington M (2013) Assessing the potential improvement in short-term earthquake forecasts from incorporation of GPS data. Geophys Res Lett 40:2631–2635

Yang C-S, Kao S-P, Lee F-B, Hung P-S (2004) Twelve different interpolation methods: a case study of Surfer 8.0. In: Paper presented at the Proceedings of the XXth ISPRS congress

Yao Y, Chen P, Wu H, Zhang S, Peng W (2012) Analysis of ionospheric anomalies before the 2011 M w 9.0 Japan earthquake. Chin Sci Bull 57:500–510

Yue H, Lay T (2011) Inversion of high-rate (1 sps) GPS data for rupture process of the 11 March 2011 Tohoku earthquake (Mw 9.1). Geophys Res Lett 38:142

Zhang Y, Jiang Z, Huang H et al (2014) Thermal anomalies detection before 2013 Songyuan earthquake using MODIS LST data. In: Paper presented at the 2014 IEEE international geoscience and remote sensing symposium (IGARSS)